



OPEN

Control of white mold (*Sclerotinia sclerotiorum*) through plant-mediated RNA interference

Philip L. Walker, Dylan J. Ziegler, Shayna Giesbrecht, Austein McLoughlin, Joey Wan, Deirdre Khan, Vanessa Hoi, Steve Whyard & Mark F. Belmonte

The causative agent of white mold, *Sclerotinia sclerotiorum*, is capable of infecting over 600 plant species and is responsible for significant crop losses across the globe. Control is currently dependent on broad-spectrum chemical agents that can negatively impact the agroecological environment, presenting a need to develop alternative control measures. In this study, we developed transgenic *Arabidopsis thaliana* (AT1703) expressing hairpin (hp)RNA to silence *S. sclerotiorum* *ABHYDROLASE-3* and slow infection through host induced gene silencing (HIGS). Leaf infection assays show reduced *S. sclerotiorum* lesion size, fungal load, and *ABHYDROLASE-3* transcript abundance in AT1703 compared to wild-type Col-0. To better understand how HIGS influences host–pathogen interactions, we performed global RNA sequencing on AT1703 and wild-type Col-0 directly at the site of *S. sclerotiorum* infection. RNA sequencing data reveals enrichment of the salicylic acid (SA)-mediated systemic acquired resistance (SAR) pathway, as well as transcription factors predicted to regulate plant immunity. Using RT-qPCR, we identified predicted interacting partners of *ABHYDROLASE-3* in the polyamine synthesis pathway of *S. sclerotiorum* that demonstrate co-reduction with *ABHYDROLASE-3* transcript levels during infection. Together, these results demonstrate the utility of HIGS technology in slowing *S. sclerotiorum* infection and provide insight into the role of *ABHYDROLASE-3* in the *A. thaliana*–*S. sclerotiorum* pathosystem.

Host-induced gene silencing (HIGS) takes advantage of the RNA interference (RNAi) pathway, which is conserved within most eukaryotic organisms^{1,2}. This pathway can be triggered by dsRNA molecules recognized and further processed into small interfering RNAs (siRNAs) by Dicer-like proteins (DCLs). These siRNAs with sequence complementarity to target pathogen transcripts are subsequently bound to Argonaute proteins (AGOs), forming the RNA induced silencing complex (RISC) with complementary siRNAs guiding the RISC to target mRNA transcripts for degradation^{3,4}. HIGS uses complementary transgene-expressed hairpin (hp)RNA that is capable of targeting a single gene's transcripts, thus removing or reducing the risk of off-target effects on the agroecological environment⁵. Applications of HIGS have demonstrated success against a diverse set of fungal pathogens, including ascomycetes *Botrytis cinerea*⁶, *Fusarium graminearum*⁷ and *Verticillium dahlia*⁸, basidiomycetes *Ustilago hordei*⁹ and *Melampsora lini*¹⁰, and oomycetes *Phytophthora infestans*¹¹ and *Hyaloperonospora parasitica*¹². Successful HIGS-mediated control of a phytopathogen is dependent on choosing a target gene whose transcript abundance can be adequately reduced by the hairpin (hp)RNA-expressing transgene^{13,14}. In prior studies, we explored the efficacy of the putative tRNA synthetase *ABHYDROLASE-3* as an RNAi candidate gene through the topical application of long dsRNA in spray-induced gene silencing (SIGS) to reduce pathogenicity of *S. sclerotiorum* on *B. napus* and *Arabidopsis thaliana*¹⁵. Significant reductions in *S. sclerotiorum* lesion progression post application of *ABHYDROLASE-3* targeting dsRNA molecules were correlated with reductions in target transcript levels as early as 24 h post infection. Subsequently, Wytinck et al.¹⁶ engineered *B. napus* to express hpRNAs targeting the *S. sclerotiorum* *ABHYDROLASE-3* through HIGS and demonstrated reduced disease severity in inoculated stem tissues, coupled with significant *ABHYDROLASE-3* transcript reduction. As *S. sclerotiorum* infection commonly initiates in leaves prior to progressing to stem tissues^{17,18}, understanding how *ABHYDROLASE-3* silencing influences the host response directly at the site of infection can provide

Department of Biological Sciences, University of Manitoba, Winnipeg, MB R3T 2N2, Canada. email: Mark. Belmonte@umanitoba.ca

insight into the control *S. sclerotiorum* prior to systemic infection. Further, while *ABHYDROLASE-3* silencing has demonstrated reduced disease severity against *S. sclerotiorum* using SIGS and HIGS technology, its role in pathogenesis is still largely unknown and identification of interacting partners and pathways may provide new candidates to target through RNAi.

Plants activate innate immunity pathways in response to pathogen attack and are dependent on the recognition of specific pathogen-derived molecules¹⁹. These pathways are commonly separated into necrotrophic and biotrophic responses and demonstrate distinct modes of pathogen detection. For example, necrotrophic pathogens are detected through the presence of pathogen and damage associated molecular patterns (PAMPs/DAMPs) via pattern recognition receptors (PRRs) in pattern-triggered immunity (PTI), while in contrast, biotrophic pathogens are detected via intracellular NBS-LRR proteins detecting secreted effector molecules in effector-triggered immunity (ETI)¹⁹. Activation of these recognition pathways induces specific defense hormones which can further activate down-stream defense processes to appropriately respond to pathogen attack. These hormones include jasmonic acid (JA) and ethylene (ET) which can directly activate the induced systemic resistance (ISR) pathway and are associated with promoting physical barriers against necrotrophic pathogens²⁰. Other phytohormones like salicylic acid (SA) activate the systemic acquired resistance pathway (SAR) leading to a local hypersensitive response as a defense against biotrophic infection^{21,22}. While *S. sclerotiorum* has been previously categorized as a necrotrophic fungal pathogen, recent reports provide evidence of an early biotrophic phase^{23,24}. *S. sclerotiorum* secretes pathogenicity factors including oxalic acid (OA) and a suite of cell wall degrading enzymes to weaken and break down host cells upon infection^{25,26}. During the initial stages of infection, a brief biotrophic phase may occur, where OA and other secreted pathogenicity factors act to suppress host defenses, specifically the SA-mediated SAR pathway^{23,24}. The inability of *S. sclerotiorum* to successfully suppress SAR may lead to increased resistance against *S. sclerotiorum* infection. Further support for this initial biotrophic phase comes from the identification of secreted effector molecules essential for pathogenicity²⁷ and intracellular NBS-LRRs necessary for successful defense against *S. sclerotiorum*²⁸. Lastly, synergistic effects between SA-mediated SAR and JA/ET-mediated ISR have been described against necrotrophic infection²⁹ and that removal of either of these defense hormones will result in an unsuccessful defense response³⁰.

In the current study, we engineered *A. thaliana* expressing hpRNA complementary to *S. sclerotiorum* *ABHYDROLASE-3* under the activity of a CaMV 35S promoter (AT35S::SS1G_01703RNAi herein referred to as AT1703). AT1703 *A. thaliana* was more tolerant to *S. sclerotiorum* infection with reduced lesion size, fungal load and *ABHYDROLASE-3* transcript abundance compared to wild-type Col-0. Light microscopy of the infection process further identified reduced epidermal and mesophyll tissue degradation and vascular tissue colonization in AT1703 lines. Global RNA sequencing revealed enrichment of the SA-mediated SAR pathway and predictive gene regulatory network analysis predicted heat shock factor (*HSPA4A*, *HSPA8*) and TGA (*TGA10*) transcription factors as putative regulators of resistance in AT1703. Analysis of *ABHYDROLASE-3* predicted interacting partners suggests this pathogenicity factor plays a role in the methionine salvage pathway which is necessary for successful polyamine biosynthesis. Taken together, these data demonstrate the utility of HIGS in slowing *S. sclerotiorum* infection and highlight the importance of the SA-mediated SAR pathway in contributing to successful defense against *S. sclerotiorum*.

Results

HIGS of *S. sclerotiorum* *ABHYDROLASE-3* slows infection in transgenic AT1703 Arabidopsis. hpRNA complementary to the *ABHYDROLASE-3* gene coding sequence of *S. sclerotiorum* (SS1G_01703) was transformed into wild-type Col-0 *A. thaliana* under the control of the CaMV 35S promoter and propagated to the T3 generation. Three independent insertion lines were propagated to the T2 generation (Supplementary Fig. S1a), and our top performing line (AT1703.1, herein referred to as AT1703) was selected for RNA sequencing and further analysis at the T3 generation due to its significantly reduced lesion size and *ABHYDROLASE-3* transcript reduction compared to wild-type Col-0 (Supplementary Fig. S1b). Light microscopy of leaf cross sections using the chitin-targeting stain lactophenol blue showed no apparent differences in uninfected AT1703 and wild-type Col-0 leaves (Fig. 1a). However, at 2 dpi, wild-type Col-0 leaves show an increased abundance of *S. sclerotiorum* in both mesophyll and vascular tissues (Fig. 1b). At 3 dpi *S. sclerotiorum* shows further colonization of vascular tissue in wild-type Col-0 compared to AT1703 leaves, coupled with decreased levels of epidermal and mesophyll tissue degradation in AT1703 lines (Fig. 1c). At 1 dpi, no differences in lesion size or fungal abundance were observed (Fig. 1d,e), while at 2 dpi, *S. sclerotiorum* *ABHYDROLASE-3* transcript levels showed a 73% reduction in AT1703 with no significant differences in lesion size or fungal load compared to wild-type Col-0 (Fig. 1f). However, by 3 dpi AT1703 showed a 48% reduction in lesion size, an 84% reduction in fungal load, and a 93% reduction in *ABHYDROLASE-3* transcript accumulation compared to wild-type Col-0 plants (Fig. 1d,f). While this significant transcript reduction is present as early as 2 dpi, these data suggest a ~24-h lag phase where transcript abundance is reduced but insufficient to immediately slow infection (Fig. 1d,f).

Global RNA-sequencing reveals enriched gene activity of the salicylic acid-mediated SAR pathway in AT1703. To uncover the underlying gene expression patterns between AT1703 and wild-type Col-0 we performed global RNA sequencing on uninfected (0 dpi) leaves as well as directly at the site of infection at mid (2 dpi) and late (3 dpi) stages of *S. sclerotiorum* leaf infection. Hierarchical clustering of raw count expression values revealed distinct clusters forming between uninfected (0 dpi) and *S. sclerotiorum* infected tissues (Fig. 2). Genotypes also clustered in response to *S. sclerotiorum* infection compared to infection time points. Global gene activity showed no significant differences in the proportion of low, moderate or highly accumulated transcripts, with on average 20%, 21% and 58% of detected transcripts showing low, moderate and high-count levels respectively (Fig. 2). Further, total transcript detection between genotypes is similar, with an increase in

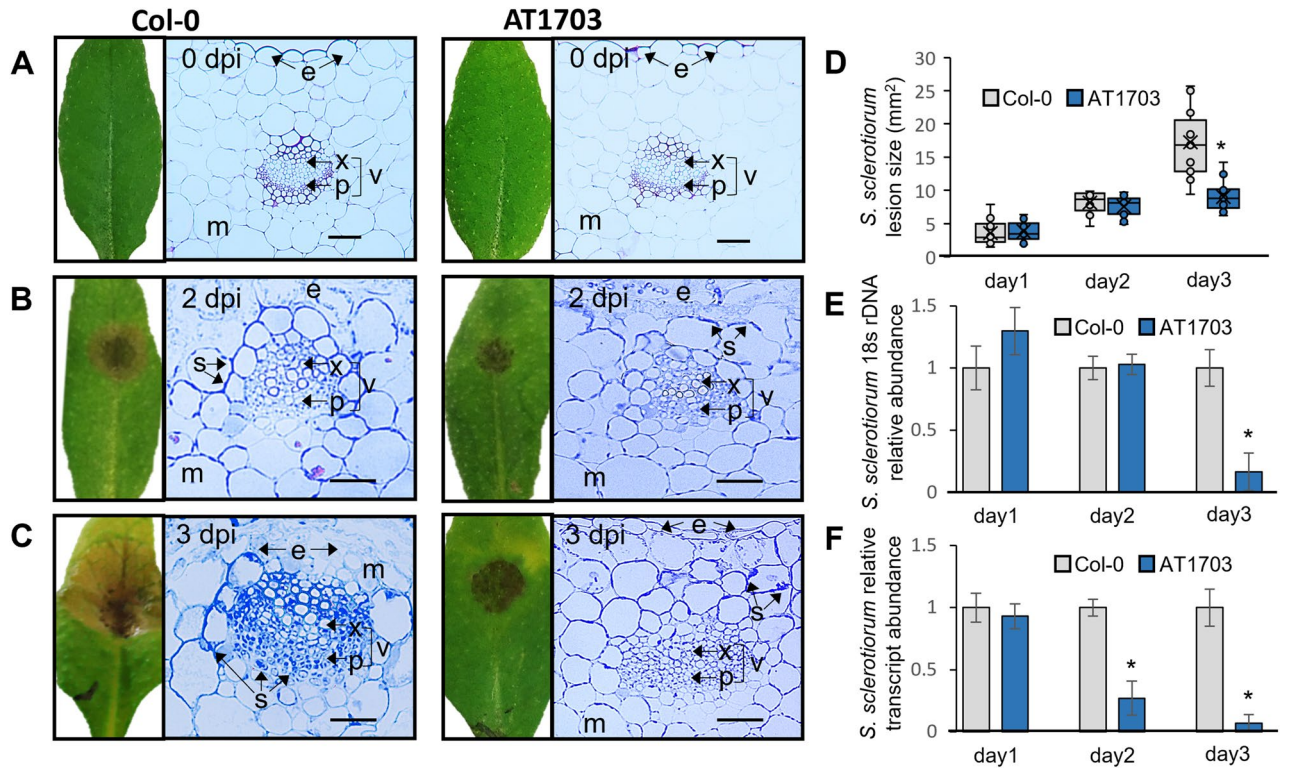


Figure 1. Whole-leaf and cross section of wild-type Col-0 and AT1703 *A. thaliana* uninfected control and infected with *S. sclerotiorum* at (A) 0, (B) 2, and (C) 3 days post inoculation. Five μm cross-sections generated using Leica RM2245 and stained with (A) toluidine blue and (B,C) lactophenol cotton blue. (D) lesion size (mm^2), (E) fungal load and (F) target transcript reduction in Col-0 and T3 AT1703 leaves infected with *S. sclerotiorum*. *A. thaliana* inoculated with $1 \times 10^6 \mu\text{L}$ ascospore solution and measured at 2- and 3-days post inoculation. (D) Sample size of $n = 15$ leaves per line were measured using ImageJ software and normalized to wild-type Col-0 leaves for lesion measurements. Error bars represent standard error and significance was determined using a Student's *t*-test ($p < 0.05$). * = significance. (E) Fungal load quantified using relative abundance of 18S *S. sclerotiorum* rDNA and calculated using ΔCT against wild-type Col-0. Each line consists of three biological replicates, each containing three infected *A. thaliana* leaves. (F) Target transcript abundance calculated using the $\Delta\Delta\text{CT}$ method with *Sac7* as a reference gene. Each line consists of three biological replicates, each containing three infected *A. thaliana* leaves for (E) and (F). Error bars represent standard error. Scale bars = 50 μm . e, epidermis; m, mesophyll; x, xylem; p, phloem; v, vasculature; s, *S. sclerotiorum*.

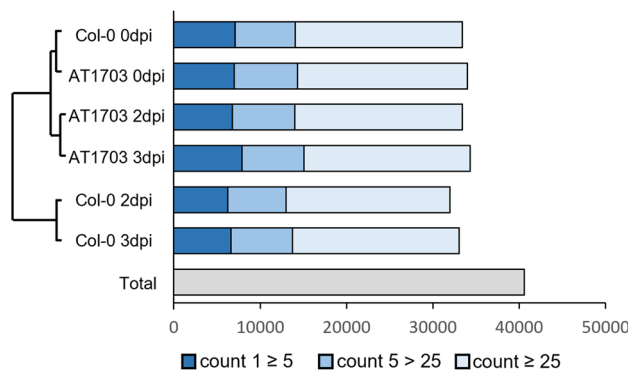


Figure 2. Global gene activity in the *A. thaliana*-*S. sclerotiorum* pathosystem. Hierarchical clustering and global gene activity of wild-type Col-0 and AT1703 at 0-, 2- and 3-days post inoculation. Number of transcripts detected across all treatments were identified through RNA sequencing. Transcripts with a count value > 1 are considered detected. Detected transcripts are subdivided into low ($1 \geq 5$), moderate ($5 > 25$), or high (≥ 25) abundance levels.

1813 and 1348 detected transcripts in AT1703 compared to Col-0 at 2 and 3 dpi respectively due to an increased abundance of *S. sclerotiorum* transcripts in wild-type Col-0.

Differential expression analysis identified shared and specifically up-regulated gene sets in response to *S. sclerotiorum* in AT1703 and wild-type Col-0 (Fig. 3a). For example, 335 and 235 genes were specifically up-regulated at 2 and 3 dpi respectively, while 444 genes were up-regulated at both timepoints in AT1703. Further, 449 and 235 genes were down-regulated in AT1703 relative to Col-0 at 2 and 3 dpi respectively, and 351 genes were down-regulated at both timepoints (Supplementary Dataset S4). Next, to identify putative biological processes associated with these differentially expressed gene sets, we performed Gene ontology (GO) term enrichment (Fig. 3b). Data show the SA-mediated SAR pathway ($p = 2.05 \times 10^{-27}$) and SA biosynthesis ($p = 1.16 \times 10^{-31}$) as well as enrichment of the hypersensitive response ($p = 3.07 \times 10^{-7}$) in gene sets up-regulated at 2 and 3 dpi in AT1703. The enrichment of SA biosynthesis, SAR and the hypersensitive response indicate a strong role of the SAR defense pathway in successful defense response and incompatible interaction ($p = 1.28 \times 10^{-13}$) found in AT1703 lines. While SA biosynthesis and SAR demonstrate shared enrichment between AT1703 at 2 and 3 dpi, it is worth noting that statistically significant enrichment is also found specifically at 2 dpi, while no such enrichment is found for down-stream activated defense processes like the hypersensitive response and incompatible interaction (Fig. 3b). Further, 750 genes were up-regulated in response to *S. sclerotiorum* across both genotypes and timepoints (Fig. 3a). This shared gene set showed significant enrichment of PTI associated JA ($p = 7.77 \times 10^{-34}$) and ET biosynthesis ($p = 1.32 \times 10^{-49}$), induced systemic resistance ($p = 6.63 \times 10^{-8}$) and PAMP induction of immune response ($p = 1.71 \times 10^{-4}$) (Supplementary Dataset S1), suggesting that activity of these JA/ET-mediated defense pathways alone in wild-type Col-0 are insufficient to slow *S. sclerotiorum* infection without enrichment of SA-mediated SAR, providing additional evidence of the synergism of SA-mediated SAR and JA/ET-mediated ISR/PTI in mounting a successful defense against *S. sclerotiorum*. In contrast, enrichment of up-regulated genes specifically in wild-type Col-0 show association with programmed cell death and cell wall reinforcement, including leaf senescence ($p = 1.97 \times 10^{-6}$), autophagy ($p = 8.88 \times 10^{-6}$), cell wall modification ($p = 2.61 \times 10^{-6}$) and organization ($p = 2.75 \times 10^{-4}$), and lignin biosynthesis ($p = 7.22 \times 10^{-7}$).

To explore potential regulators of immunity in AT1703 expressed throughout infection, we performed a transcription factor network analysis using SeqEnrich in our AT1703 up-regulated gene set in response to *S. sclerotiorum*. Here, we identified the TGA transcription factor *TGA10*, as well as the HSFs transcription factors *HSA4A* and *HSA8*, which are both predicted to regulate SA-signalling and SAR activity (Fig. 4a). Further, we explored differential expression between AT1703 and wild-type Col-0 in response to *S. sclerotiorum* in genes that have been previously described to interact with these transcription factors. Here, we found up-regulation of the TGA interacting *ENHANCED DISEASE SUSCEPTIBILITY 1 (EDS1)*, *NONEXPRESSER OF PR GENES 1 (NPR1)* and *ISOCHORISMATE SYNTHASE 1 (ICS1)* in AT1703 *A. thaliana*, as well as up-regulation of the *HSA4A* interacting kinase *MITOGEN-ACTIVATED PROTEIN KINASE 3 (MPK3)* (Fig. 4b).

ABHYDROLASE-3 silencing influences expression of polyamine synthase genes in *S. sclerotiorum*. While AT1703 demonstrates significant *ABHYDROLASE-3* transcript reduction during *S. sclerotiorum* infection, we had yet to explore the influence of *ABHYDROLASE-3* silencing on gene expression within the fungus itself. Three predicted interacting partners of *ABHYDROLASE-3* (SS1G_02233, SS1G_14434, SS1G_03597) were identified in *S. sclerotiorum* using stringdb (<https://string-db.org/>) (Fig. 5a). While SS1G_14434 and SS1G_03597 have yet to be significantly characterized, SS1G_02233 encodes a 5'-methylthioadenosine phosphorylase (MTAP) that prevents accumulation of the polyamine biosynthesis by-product S-methyl-5'-thioadenosine (MTA), inhibiting polyamine biosynthesis and ultimately fungal growth^{31,32}. Here, all three predicted interacting partners showed significant transcript reduction in *S. sclerotiorum* that was infecting AT1703 compared to wild-type Col-0 at 2 and 3 dpi (Fig. 5b). Further, reduction in these predictive partners was consistent with our target gene *ABHYDROLASE-3*, showing at least a 50% increase in reduction from 2 to 3 dpi. To further support the role of *ABHYDROLASE-3* in polyamine biosynthesis, we quantified expression of genes encoding the rate-limiting enzyme in polyamine biosynthesis *ORNITHINE DECARBOXYLASE (ODC)* as well as down-stream enzymes *SPERMINE SYNTHASE* and *SPERMIDINE SYNTHASE*. Transcript reduction was observed for all three genes in *S. sclerotiorum* challenging AT1703, suggesting a role of *ABHYDROLASE-3* in polyamine biosynthesis during *S. sclerotiorum* infection.

AT1703 is not tolerant to the phytopathogen *Botrytis cinerea*. *ABHYDROLASE-3* targeting hpRNA expressed by AT1703 was carefully designed to not share 21-nt siRNAs with transcripts of related species including the closely related necrotrophic pathogen *B. cinerea*. To study whether AT1703 was also tolerant to *B. cinerea*, we next inoculated both wild-type Col-0 and AT1703 with *B. cinerea* spores (Fig. 6a). Here, no significant differences in lesion size (Fig. 6b), fungal load (Fig. 6c) or target transcript abundance (Fig. 6d) were found using the *B. cinerea* *ABHYDROLASE-3* homolog BC1G_08022, suggesting no off-target effects in *B. cinerea* challenging AT1703.

Discussion

RNAi technology has the demonstrated ability to control pathogenic fungi in host plants through constitutively expressed dsRNA molecules in transgenic plants via host-induced gene silencing (HIGS). The constitutive expression of fungal-targeting dsRNAs allows for a durable means of protection against pathogen attack throughout the host plant lifecycle^{16,33,34}. Protection of the plant relies on successful uptake and processing of dsRNA and processed siRNAs which can be generated in the host prior to uptake by the challenging pathogen³. Cross-kingdom trafficking of both dsRNAs and processed siRNA has been demonstrated across the host-pathogen interface in necrotrophic pathogens including *S. sclerotiorum* and the closely related *B. cinerea*, making these species ideal

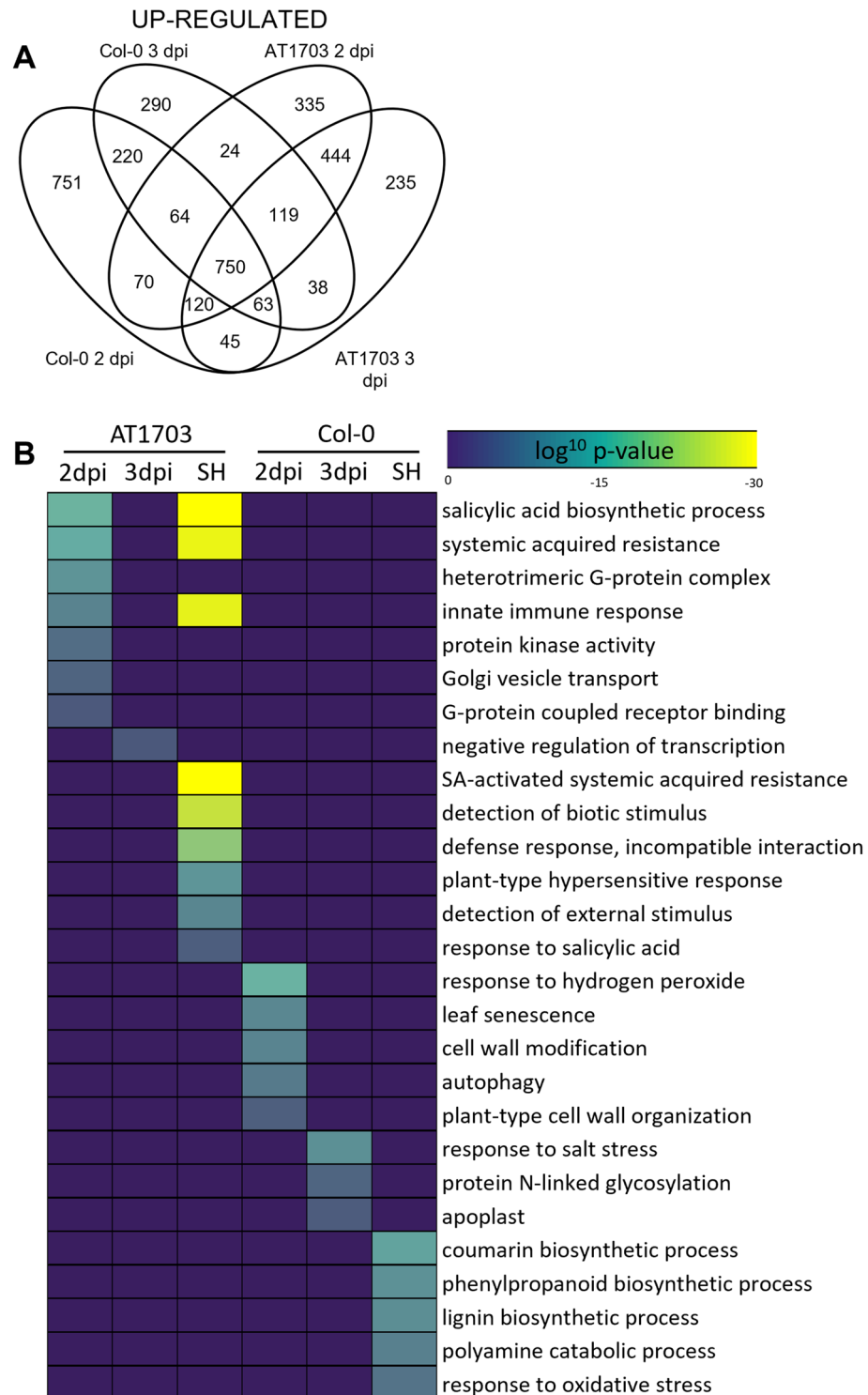


Figure 3. Identification of differentially expressed genes and enriched GO terms in response to *S. sclerotiorum* infection in wild-type Col-0 and AT1703. **(A)** Venn diagram representing up-regulated genes in infected wild-type Col-0 and AT1703 *A. thaliana*. **(B)** Heatmap of enriched GO terms associated with shared up-regulated gene patterns. GO terms considered statistically significant with a hypergeometric log₁₀ p-value < 0.001. *SH* shared.

candidates for control through RNAi^{35,36}. Here, we engineered *A. thaliana* expressing hpRNA molecules complementary to the previously identified *ABHYDROLASE-3* in *S. sclerotiorum*.

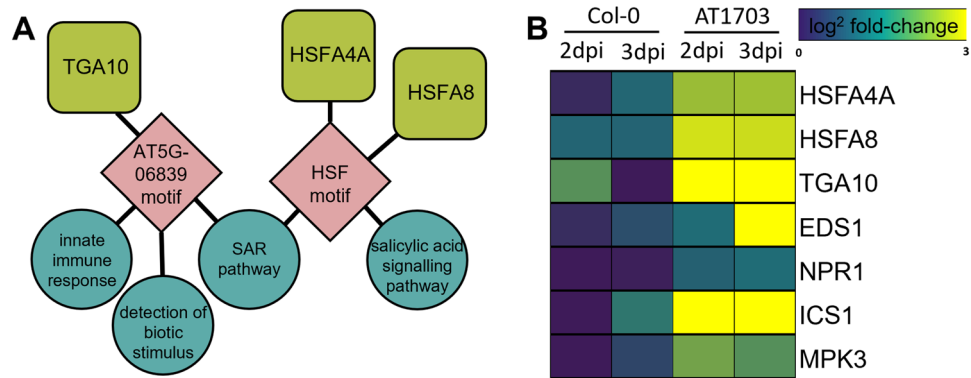


Figure 4. Differential expression and transcription factor network analysis of up-regulated shared AT1703 gene set in response to *S. sclerotiorum*. **(A)** Predictive transcription factor network analysis in shared AT1703 shared gene set in response to *S. sclerotiorum*. Yellow-green rounded squares represent significantly up-regulated transcription factors identified in AT1703 gene set, pink diamonds represent transcription factor DNA binding motifs, teal circles represent GO terms, and edges between DNA motifs and GO terms represent enriched motif sequences involved in the regulation of the GO term. **(B)** Log² fold change of infected AT1703 and wild-type Col-0 at 2- and 3-days post inoculation relative to respective uninfected treatments.

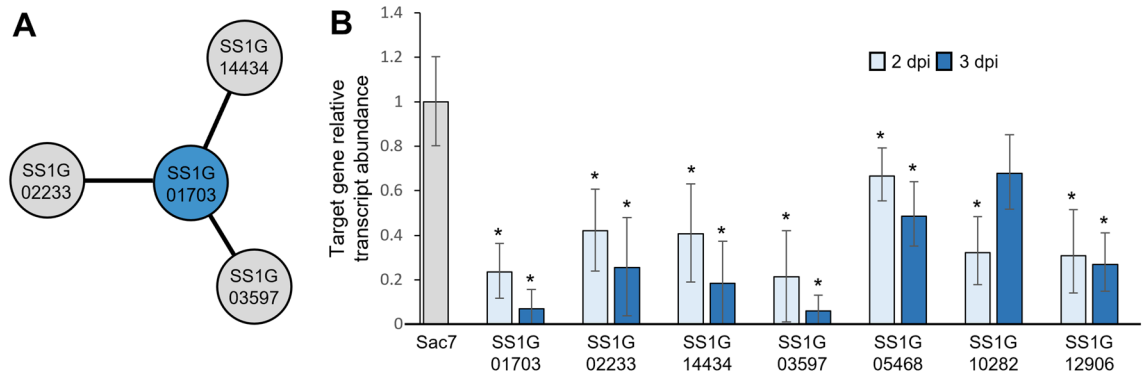


Figure 5. Transcript abundance of *ABHYDROLASE-3* (SS1G_01703) predicted interacting partners using RT-qPCR. **(A)** predictive interacting network of *ABHYDROLASE-3* generated through Stringdb based on gene fusion and co-expression analyses. **(B)** RT-qPCR target transcript abundance of predicted interacting partners in *S. sclerotiorum* challenging AT1703 *A. thaliana* at 2- and 3-days post inoculation relative to wild-type Col-0. Target transcript abundance calculated using the $\Delta\Delta CT$ method with *Sac7* as a reference gene. Each line consists of three biological replicates, each containing three infected *A. thaliana* leaves. Error bars represent standard error and significance was determined using a Student's *t*-test ($p < 0.05$) with a Bonferroni correction. *Significance.

Successful *S. sclerotiorum* infection involves the penetration and destruction of host epidermis and mesophyll tissue followed by colonization of the vasculature^{28,37}. Once the vascular tissue has been colonized, infection is considered systemic, being able to cut off host nutrient supply while the fungus extends mycelia conveniently throughout host tissues. Susceptible genotypes have demonstrated preferential growth throughout the vascular tissue in *Brassica* species compared to respective tolerant lines³⁸. While microscopy of *S. sclerotiorum* infected wild-type Col-0 and AT1703 demonstrates reduced *S. sclerotiorum* abundance in AT1703, we also find decreased levels of epidermal and mesophyll tissue degradation and reduced abundance of vascular tissue fungal colonization, thereby preventing systemic infection throughout the plant. Limiting systemic infection has significant implications on reducing yield losses from *S. sclerotiorum* infection. This was demonstrated by Wytinck et al.¹⁶, where transgenic *B. napus* lines expressing the same *ABHYDROLASE-3* hpRNA construct against *S. sclerotiorum* show reduced vascular tissue colonization coupled with an increase in seed mass compared to untransformed *B. napus* post whole-plant *S. sclerotiorum* infection. As infection typically initiates on mature leaves before progressing into stem tissue through the vascular system^{39,40}, it is critical to reduce vascular colonization directly at the site of infection, which can ultimately slow *S. sclerotiorum* progression throughout the host.

Target gene silencing in the pathogen is essential to slow the infection through HIGS. AT1703 plants demonstrate significant *ABHYDROLASE-3* transcript reductions in *S. sclerotiorum* at 1 and 2 dpi, while reduced lesion size and fungal load are only identified at 3 dpi relative to wild-type Col-0 plants. Wytinck et al.¹⁶ showed similar results in transgenic *B. napus*, with significant reductions in *ABHYDROLASE-3* transcript abundance and fungal load observed at 1 and 2 dpi respectively. In contrast, prior HIGS studies targeting *S. sclerotiorum*

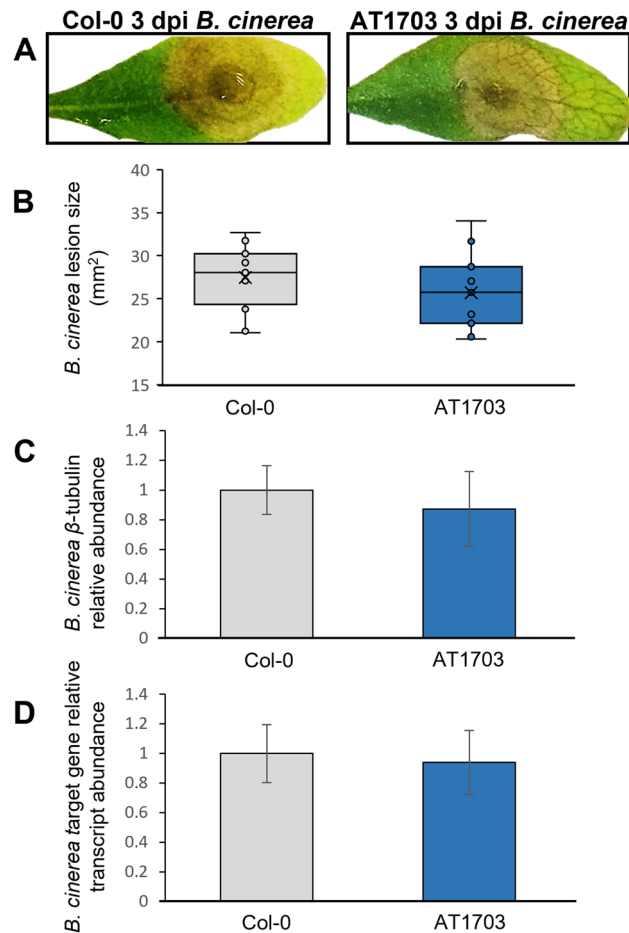


Figure 6. Lesion size (mm²), fungal load and target transcript knock down in wild-type Col-0 and T3 transgenic AT1703 *A. thaliana* leaves infected with *B. cinerea*. *A. thaliana* inoculated with 1×10^6 μ L ascospore solution and measured at 3 days post inoculation. **(B)** Sample size of $n = 15$ leaves per line were measured using ImageJ software and normalized to wild-type Col-0 leaves for lesion measurements. Error bars represent standard error and significance was determined using a Student's *t*-test ($p < 0.05$). **(C)** Fungal load quantified using relative abundance of *B. cinerea* β -tubulin and calculated using Δ CT against wild-type Col-0. Each line consists of three biological replicates, each containing three infected *A. thaliana* leaves. **(D)** Target transcript knockdown calculated using the Δ CT method with β -tubulin as a reference gene. Each line consists of three biological replicates, each containing three infected *A. thaliana* leaves for **(C)** and **(D)**. Error bars represent standard error.

essential genes (*TRX1*, *OA*) detected both target transcript reduction and reduced lesion size at 2 dpi in host plants^{33,41}, suggesting this delay to be specific to HIGS plants targeting *ABHYDROLASE-3*. These findings may be attributed to down-stream interactions of *ABHYDROLASE-3* with other interacting partners. Reduced activity of *ABHYDROLASE-3* in addition to regulators of polyamine biosynthesis are likely responsible for or at least contribute to the inhibition of fungal growth. However, further characterization of *ABHYDROLASE-3* interacting partners and the polyamine biosynthesis pathway during *ABHYDROLASE-3* silencing are required to better understand this delay.

While the utility of HIGS in controlling *S. sclerotiorum* has been demonstrated in multiple host plants^{16,33,34}, the underlying host response of these transgenic plants, as well as host–pathogen interactions in this system are less understood and dependent upon the specific gene being silenced. Here, global RNA sequencing and differential expression analyses provide insight into the response of AT1703 leaves to *S. sclerotiorum* directly at the site of infection. Moreover, the mode of pathogenicity of *S. sclerotiorum* has been recently debated, as emerging studies have suggested the presence of a brief biotrophic stage during early infection highlighted by the suppression of the SA-mediated SAR pathway^{23,24}. SA biosynthesis in response to pathogen attack occurs through the isochorismate synthase (ICS) pathway, where *ICS1* is essential for SA biosynthesis and successful SAR⁴². Downstream of SA accumulation, *NPR1* activity is required for expression of pathogenesis-related (*PR*) genes involved in the SAR response through SA signal transduction^{42,43}. AT1703 shows significant enrichment of the SA-mediated SAR pathway compared to wild-type Col-0, with enrichment of both *ICS1* and *NPR1* in response to *S. sclerotiorum* infection, suggesting an inability to suppress SAR while infecting AT1703 *A. thaliana*. Further, while *NPR1* does not contain a DNA binding domain, it acts as a transcriptional cofactor, enhancing TGA transcription factor

binding affinity to *PR* genes upon translocation into the nucleus in response to SA⁴⁴. While multiple TGA transcription factors have been shown to interact with *NPR1* in response to SA in *A. thaliana*⁴⁵, *TGA10* interaction has yet to be explored. Here, *TGA10* was identified as the lone member of the TGA transcription factor family significantly enriched in AT1703 *A. thaliana* in response to *S. sclerotiorum* and was identified in our predictive transcription factor network to regulate SAR activity. Further, *TGA10* has been demonstrated to be necessary for activation of reactive oxygen species (ROS) response in PTI in response to the bacterial PAMP flg22, where *tga10* mutants were unable to activate flg22-response genes and showed reduced ROS production⁴⁶, highlighting its importance in the activation of defense genes in response to pathogen attack. Our network analysis further identified two HSF transcription factors (*HSA44A*, *HSA8*) associated with the SA signalling pathway that are up-regulated in AT1703 in response to *S. sclerotiorum*. While HSFs have been shown to interact directly with *EDS1*, resulting in SA accumulation in response to pathogen attack^{47,48}, similarly to *TGA10*, *HSA44A* and *HSA8* have specifically been implicated in the host ROS response as well as activation of the host antioxidant system^{49,50}. Activation of these HSFs can act through phosphorylation by *MPK3* in response to stress, which also demonstrates significant up-regulation in AT1703 *A. thaliana* in response to *S. sclerotiorum*^{49,51,52}.

While these data suggest SAR activity is an essential component of a successful defense response against *S. sclerotiorum* infection, SAR alone is insufficient to protect the host, as quantitative disease resistance is complex and requires the coordination of multiple defense pathways and processes⁵³. For example, SA-mediated SAR and JA/ET regulated ISR pathways exhibit synergistic effects in defense against necrotrophic pathogen attack²⁹. This was demonstrated using *npr1* knockout Arabidopsis mutants deficient in SA signalling, *coi1* mutants deficient in JA signalling, and *ein2* deficient in ET signalling, which all show hyper-susceptibility phenotypes due to the inactivity of SAR and ISR pathways³⁰. Differential expression analysis not only identified enrichment of SA-mediated SAR in AT1703, but also JA/ET biosynthesis and the ISR pathway which were significantly enriched in both AT1703 and wild-type Col-0 lines relative to their respective uninfected leaves, suggesting both defense pathways are essential in mounting a successful defense response against *S. sclerotiorum*.

To better understand the different defense responses to infection by wild-type Col-0 and AT1703 plants, we further explored defense processes enriched specifically in wild-type Col-0 and not AT1703. *S. sclerotiorum* demonstrates necrotrophic growth, especially at later stages of infection. Thus, the bi-products of gene activity belonging to autophagy and leaf senescence found in wild-type Col-0 can serve as nutrients for the progressing pathogen to continue growth as it feeds on necrotic host tissue^{54,55}. With increased necrotic host tissue available to *S. sclerotiorum* in wild-type Col-0, host plants would require mechanical defenses through cell wall reinforcement and lignification in response to cell wall degrading enzymes being consistently secreted during actively progressing infection⁵⁶. Lignification in response to *S. sclerotiorum* has previously been described by Höch et al.⁵⁶, where genes associated with lignin biosynthesis showed significantly increased expression levels in susceptible *B. napus* lines compared to moderately resistant lines, specifically during mid to late stages of infection. These findings agree with our data where we find enrichment of lignin biosynthesis and cell wall reinforcement in wild-type Col-0 lines compared to AT1703 throughout *S. sclerotiorum* infection.

While we have examined the influence *ABHYDROLASE-3* silencing has on the host response, there is also a need to explore differences within the pathogen and the effect that *ABHYDROLASE-3* silencing has at the molecular level. *ABHYDROLASE-3* is annotated as a tRNA synthetase but also predicted to be involved in aflatoxin biosynthesis. However, this gene has yet to be further characterized beyond its ability to slow *S. sclerotiorum* infection through SIGS and HIGS RNAi treatments^{15,16}. Using the stringdb (<https://string-db.org/>) protein-protein interaction network database, we identified three predictive interacting partners of *ABHYDROLASE-3* (SS1G_14434, SS1G_03597 and SS1G_02233). Expression levels of *ABHYDROLASE-3* and these predicted interacting partners in *S. sclerotiorum* were coordinately reduced in transgenic AT1703 compared to wild-type Col-0. While SS1G_14434 and SS1G_03597 have yet to be functionally characterized in *S. sclerotiorum*, SS1G_02233 encodes MTAP, which plays a critical role in cleaving and processing accumulated MTA, a by-product of polyamine biosynthesis^{31,32}. Buildup of MTA through inactivity of MTAP ultimately results in the inhibition of polyamine biosynthesis^{31,32}. This in turn can have significant impacts on fungal growth, as the three most widely distributed polyamines, putrescine, spermidine and spermine have been shown to be necessary for successful growth and cell differentiation^{32,37}. The ornithine decarboxylase (SS1G_05468) is an essential enzyme of polyamine biosynthesis, converting ornithine into the polyamine putrescine^{32,37}. Once ornithine is converted into putrescine, there are further down-stream synthase genes necessary for conversion into both spermine and spermidine. These enzymes include spermine synthase (SS1G_12906) to convert putrescine into spermine, and spermidine synthase (SS1G_10282) to convert spermine into spermidine. Our RT-qPCR analysis of these essential polyamine synthesis genes shows transcript reduction during *S. sclerotiorum* infection of AT1703 plants compared to their wild type susceptible counterparts, suggesting a potential interaction between *ABHYDROLASE-3* and the identified predictive partners of the polyamine biosynthesis pathway. Further, as putrescine can also be produced through spermine and spermidine catabolism, expression of rate limiting enzymes SSAT and PAO can also be explored to improve our understanding of *ABHYDROLASE-3* influence on polyamine metabolism³². While the potential direct or indirect interaction of *ABHYDROLASE-3* and these predictive interacting partners is still unclear, these data provide some preliminary insights of the role *ABHYDROLASE-3* plays in *S. sclerotiorum* pathogenicity and further identifies a group of promising RNAi candidate genes through the polyamine synthesis pathway.

One benefit of RNAi and HIGS technology in crop protection is the ability to design pathogen specific molecules that are ineffective against potentially beneficial species in the ecosystem^{4,58}. This requires the careful design of target sequences within genes, as dsRNA molecules containing as few as three overlapping 21-mer nucleic acid sequences have demonstrated the ability to significantly reduce off-target transcripts⁵⁹. *B. cinerea* serves as an ideal candidate to study these potential off-target effects in controlling *S. sclerotiorum* given both pathogens share similar hosts and disease cycles in addition to having a high level of sequence homology^{60,61}.

McLoughlin et al.¹⁵ showed that dsRNA targeting the *ABHYDROLASE-3* *B. cinerea* homolog BC1G_08022 was able to reduce *B. cinerea* lesion size, fungal load and BC1G_08022 transcript abundance when applied to *B. napus* leaves prior to *B. cinerea* inoculation. While BC1G_08022 is capable of slowing *B. cinerea* infection when targeted, our dsRNA region targeting *S. sclerotiorum* *ABHYDROLASE-3* shows no 21-mer overlapping regions with off-target species (Supplementary Dataset S2) and AT1703 *A. thaliana* challenged with the closely related necrotrophic fungal pathogen *B. cinerea* shows no significant differences in lesion size, fungal load or BC1G_08022 transcript reduction.

Taken together, these data demonstrate the efficacy of HIGS as an alternative control measure in slowing *S. sclerotiorum* infection through targeted silencing of *S. sclerotiorum* *ABHYDROLASE-3*. Reduction of *ABHYDROLASE-3* in *S. sclerotiorum* provides *A. thaliana* the ability to increase innate defense responses through SA-mediated SAR at the global mRNA level. The identification of co-silenced *ABHYDROLASE-3* interacting partners further uncovers a promising group of candidates for RNAi control against fungal pathogens. Finally, with ongoing concerns of potential off-target effects in RNA-based applications, we demonstrate the specificity of HIGS targeting *S. sclerotiorum* in AT1703 to a closely related fungus. Taken together, we provide evidence that HIGS applications can be used as an effective and sustainable strategy in crop improvement against necrotrophic pathogens.

Methods

Generation of transgenic *Arabidopsis*. DNA constructs consisted of a CaMV-35S promoter driving expression of a sense and antisense SS1G_01703 gene fragment separated by an intron region to form hpRNA post transcription. Cloning of this construct into *Agrobacterium tumefaciens* followed the Gateway cloning protocol (Invitrogen, Carlsbad, CA, US) using primers found in Supplementary Dataset S3 and following the methods of¹⁶. Target gene sequences were amplified using Phusion Taq (Thermo Scientific, Waltham, MA, US) under the following conditions: 98 °C for 30 s; 35 cycles of: 98 °C for 10 s, 57 °C for 30 s, and 72 °C for 30 s; and a final extension of 72 °C for 5 min. Amplicons were gel purified (New England Biolabs, Ipswich, MA, US) and digested using FastDigest *KpnI* and *XhoI* (Thermo Scientific, Waltham, MA, US) according to the manufacturer's protocols. Initially, gene fragments were ligated into the pENTR4 vector before insertion into the pHellsgate8 destination vector. To confirm insert identity, entry vectors were sequenced at the Centre for Applied Genomics in Toronto, Ontario. Inserts were then recombined into the destination vector using a Gateway LR clonase reaction (ThermoFisher Scientific) following the manufacturer's instructions, with the modification of adding 4:1 entry vector to destination vector ratio according to Wytinck et al.¹⁶. A cold shock treatment was used to transform *Agrobacterium*. Successful transformants were selected using colony PCR with *XhoI* and *XbaI* separate restriction enzyme digestions. Cultures of *Agrobacterium* were grown to OD 1.6–2.0, pelleted using centrifugation, and re-suspended in MS media and 0.001% Silwet L-77. To transform *A. thaliana*, seeds were initially sterilized using alternating washes of 70% and 95% ethanol then placed on Murashige and Skoog (MS) media (Sigma Aldrich). Seeds were vernalized for three days at 4 °C prior to being grown in a constant light incubator. Upon formation of first leaves *A. thaliana* seedlings were transplanted into Sunshine Mix #1 and grown to maturity at 22 °C. Mature flowering *A. thaliana* plants were dipped into the *Agrobacterium* culture and kept in high humidity conditions for two days. Floral dips were repeated five times before seeds were dried and harvested. Transformants were selected using MS and 150 µg/mL kanamycin media⁶². PCR was used to confirm the presence of the *S. sclerotiorum* gene using the same primers used for cloning within the plant (Supplementary Dataset S3). Three confirmed independently transformed *A. thaliana* lines were grown to the T2 generation and tested for their ability to silence *ABHYDROLASE-3* transcripts and slow *S. sclerotiorum* infection. The top performing line (AT1703.1) was subsequently selected for further RNA sequencing analysis.

***Arabidopsis thaliana* infection assays.** *Sclerotinia sclerotiorum* ascospores were collected at the Morden Research and Development Centre, Agriculture and Agri-Food Canada, Morden, MB, Canada and stored at 4 °C in desiccant in the dark according to Ref.¹⁵. *S. sclerotiorum* ascospore inoculum was made by suspending a 1×10^6 spore/mL concentration of spores in a potato dextrose broth (PDB) and peptone solution (24 g PDB, 10 g peptone, 1 L water). Using a pipette, 10 µL of the solution was transferred onto mature transgenic and wild-type Col-0 *A. thaliana* leaves at a n = 15 leaves per treatment. Plants were stored in growth chambers at room temperature (21.0 °C), with plant trays being sealed with lids to maintain high levels of humidity for three days, allowing for infection progression in planta. At 2- and 3-days post inoculation (dpi), lesion area was quantified using ImageJ software and leaves were collected for RNA sequencing, fungal load, and transcript abundance experiments. Fifteen infection sites were quantified per treatment while three leaves were collected per bio-replicate with three biological replicates collected per treatment. *Botrytis cinerea* infections were performed using ascospores from the Saint-Jean sur Richelieu Research and Development Centre, Agriculture and Agri-Food Canada, QC, Canada following the same protocol for *S. sclerotiorum* ascospore inoculations.

DNA extraction and plant genotyping. Two-week-old *A. thaliana* leaves were collected and ground using a GenoGrinder 2000 (Spex CertiPrep, Metuchen, New Jersey, USA). DNA was extracted according to Wytinck et al.¹⁶ with DNA extraction buffer [0.25 M NaCl, 1 M 2-amino-2-(hydroxymethyl)-1,3-propanediol (TRIS)-HCl pH 7.5, 25 mM EDTA pH 8, 0.5% SDS]. DNA was precipitated with isopropanol and subsequently washed with 75% ethanol before being dissolved in water. PCR was performed using GoTaq Green Master Mix (Promega, Madison WI, USA) according to manufacturer's instructions using *ABHYDROLASE-3* specific primers (Supplementary Dataset S3). Thermocycler conditions were 94 °C for 2 min, followed by 35 cycles of: 94 °C for 1 min, 56 °C for 30 s, 72 °C for 35 s, and a final extension at 72 °C for 5 min. PCR products were then loaded on a 1% agarose gel containing ethidium bromide with 2 µL of sample loaded per well against FastRuler

Middle Range DNA Ladder (Thermo Fisher) as a reference. Gels were visualized under UV light using the Axigen[®] Gel Documentation System (Axigen, Corning, NY, US).

Lactophenol cotton blue stain microscopy. *Arabidopsis thaliana* leaf tissue was embedded in historesin (Leica, Wetzlar, GER) and vacuum infiltrated in 2.5% glutaraldehyde and 1.6% paraformaldehyde fixative solution. Methylcellulosolve (Sigma-Aldrich, St. Louis, MO, USA) was used to remove pigment followed by three transfers of 100% ethanol, one every 24 h to dehydrate tissue. Tissue was then infiltrated with historesin during a 3-day period of increasing concentrations of resin. Day 1: 1:3 historesin:100% alcohol, day 2: 2:3 historesin:100% alcohol, and day 3: 100% historesin. Tissue was then embedded in blocks with an embedding solution of activated historesin, hardener and polyethylene glycol according to Wytinck et al.¹⁶. Sections were cut at 5 μ m with a Leica RM2245 microtome and *S. sclerotiorum* infected tissues stained with lactophenol cotton blue for 20 min, while uninfected 0 days post inoculated tissues were stained with 0.1% toluidine blue O for 15 min. Uninfected and infected wild-type Col-0 and AT1703 *A. thaliana* leaves were imaged using a Leica DFC450C camera.

RT-qPCR analysis. *Sclerotinia sclerotiorum* and *B. cinerea* RT-qPCR primers were designed using Primer3 (<http://bioinfo.ut.ee/primer3/>) and subsequently validated using the Primer BLAST tool (www.ncbi.nlm.nih.gov/tools/primer-blast) with a product range of 70–90 bp, GC% range of 40–60% and a primer size range of 18–23 bp. Transcript abundance was measured on the Bio-Rad CFX96 Connect Real-Time system using SsoFast EvaGreen Supermix (Bio-rad Laboratories, Hercules, CA, US) in 10 μ L reactions according to manufacturer's protocol using the following conditions: 95 °C for 30 s, and 45 cycles of: 95 °C for 2 s and 60 °C for 5 s. Melt curves were performed at a range of 65–95 °C with 0.5 °C increments to assess nonspecific amplification and primer dimers. Relative transcript accumulation was calculated using the $\Delta\Delta$ Ct method⁶³, relative to *Sac7* (SS1G_12350) for *S. sclerotiorum* and *tubA* (BC1G_00122) for *B. cinerea* using three biological replicates per treatment and three technical replicates per biological replicate. The same $\Delta\Delta$ Ct method was used to quantify expression levels of RNAi machinery in *S. sclerotiorum* and have been used and validated in Refs.^{15,16}. All RT-qPCR primers used in this study can be found in Supplementary Dataset S3.

mRNA library preparation and RNA sequencing. RNA was isolated using the Ambion[®] RNaqueous[®] micro kit (ThermoFisher Scientific) according to manufacturer's instructions. RNA quality was analyzed using the Agilent 6000 Pico LabChip[®] and Agilent 2100 Bioanalyzer software (Agilent Technologies, USA). RNA quantity was determined using the Quant-iT[™] RiboGreen[®] kit (ThermoFisher Scientific) according to manufacturer's instructions. NEBNext Oligo d(T)₂₅ beads (New England BioLabs, Ipswich, MA, USA) were used for mRNA purification. cDNA library synthesis was performed according to Ziegler et al.⁶⁴ with three biological replicates per treatment each containing three *A. thaliana* leaves. Subsequently, 100 bp paired-end RNA sequencing was performed on the Illumina HiSeq4000 platform (Génome Québec Innovation Centre, McGill University, Montreal, Canada).

RNA sequencing analysis. Raw and processed sequence reads were deposited at the Gene Expression Omnibus under the accession GSE217513. Read quality control and adapter sequence removal was performed using Trimmomatic 0.36⁶⁵ (HEADCROP:9 LEADING:30 TRAILING:30 SLIDINGWINDOW:4:30 MINLEN:50). Surviving reads were aligned to the TAIR10 *A. thaliana* genome using HISAT2⁶⁶ alignment software. Raw count data was generated using featureCounts⁶⁷ and inputted into pvclust (<https://cran.r-project.org/web/packages/pvclust/index.html>) for hierarchical clustering analysis with a detection cutoff ≥ 1 . Detected transcripts were subsequently sorted into low ($1 \geq 5$), moderate ($5 > 25$), or high (≥ 25) abundance levels. Further, raw count data was processed in DESeq2 for differential expression analysis. Here, differentially expressed genes (DEGs) were identified between pairwise comparisons at a p-value cutoff of $p < 0.0001$. GO enrichment of identified DEGs was performed using SeqEnrich⁶⁸ with terms being considered significantly enriched at $p \leq 0.001$ according to software specifications. GO heatmap visualization was performed using the conditional formatting function in Excel. GO summary tables can be found in Supplementary Dataset S1. Predictive transcription factor networks were generated using SeqEnrich (Supplementary Dataset S5) with DEG gene lists being used as input. Networks were subsequently visualized using Cytoscape 3.9.1. software (<https://cytoscape.org/>).

Data availability

All RNA sequencing data are available at the Gene Expression Omnibus (GEO) data repository (GSE217513).

Received: 28 November 2022; Accepted: 11 April 2023

Published online: 20 April 2023

References

1. Gutbrod, M. J. & Martienssen, R. A. Conserved chromosomal functions of RNA interference. *Nat. Rev. Genet.* **21**, 311–331 (2020).
2. Agrawal, N. et al. RNA interference: Biology, mechanism, and applications. *Microbiol. Mol. Biol. Rev.* **67**, 657–685 (2003).
3. Koch, A. & Wassenegger, M. Host-induced gene silencing—Mechanisms and applications. *New Phytol.* **231**(1), 54–59 (2021).
4. Zand Karimi, H. & Innes, R. W. Molecular mechanisms underlying host-induced gene silencing. *Plant Cell* **34**(9), 3183–3199 (2022).
5. Christiaens, O. et al. Literature review of baseline information on RNAi to support the environmental risk assessment of RNAi-based GM plants. *EFSA Support. Publ.* **15**(5) (2018).
6. Patel, R. M., van Kan, J. A., Bailey, A. M. & Foster, G. D. RNA-mediated gene silencing of superoxide dismutase (*bcsod1*) in *Botrytis cinerea*. *Phytopathology* **98**, 1334–1339 (2008).

7. McDonald, T., Brown, D., Keller, N. P. & Hammond, T. M. RNA silencing of mycotoxin production in *Aspergillus* and *Fusarium* species. *Mol. Plant Microbe Interact.* **18**, 539–545 (2005).
8. Song, Y. & Thomma, B. P. H. J. Host-induced gene silencing compromises *Verticillium wilt* in tomato and *Arabidopsis*. *Mol. Plant Pathol.* **19**(1), 77–89 (2018).
9. Laurie, J. D., Linning, R. & Bakkeren, G. Hallmarks of RNA silencing are found in the smut fungus *Ustilago hordei* but not in its close relative *Ustilago maydis*. *Curr. Genet.* **53**, 49–58 (2008).
10. Lawrence, G. J., Dodds, P. N. & Ellis, J. G. Transformation of the flax rust fungus, *Melampsora lini*: Selection via silencing of an avirulence gene. *Plant J.* **61**, 364–369 (2010).
11. Latijnhouwers, M. & Govers, F. A *Phytophthora infestans* G-protein beta subunit is involved in sporangium formation. *Eukaryot. Cell* **2**, 971–977 (2003).
12. Gaulin, E. *et al.* The CBEL glycoprotein of *Phytophthora parasitica var-nicotianae* is involved in cell wall deposition and adhesion to cellulosic substrates. *J. Cell Sci.* **115**, 4565–4575 (2002).
13. Rajam, M. V. & Chauhan, S. Host-induced gene silencing (HIGS): An emerging strategy for the control of fungal plant diseases. In *Genome Engineering for Crop Improvement. Concepts and Strategies in Plant Sciences* (eds Sarmah, B. K. & Borah, B. K.) 97–116 (Springer, 2021).
14. Nunes, C. C. & Dean, R. A. Host-induced gene silencing: A tool for understanding fungal host interaction and for developing novel disease control strategies. *Mol. Plant Pathol.* **13**(5), 519–529 (2012).
15. McLoughlin, A. G. *et al.* Identification and application of exogenous dsRNA confers plant protection against *Sclerotinia sclerotiorum* and *Botrytis cinerea*. *Sci. Rep.* **8**(1), 7320 (2018).
16. Wytinck, N. *et al.* Host induced gene silencing of the *Sclerotinia sclerotiorum* ABHYDROLASE-3 gene reduces disease severity in *Brassica napus*. *PLoS One.* **17**(8), (2022).
17. Shahoveisi, F., Riahi Manesh, M. & del Río Mendoza, L. E. Modeling risk of *Sclerotinia sclerotiorum*-induced disease development on canola and dry bean using machine learning algorithms. *Sci. Rep.* **12**, 864 (2022).
18. Jamaux, I., Gélie, B. & Lamarque, C. Early stages of infection of rapeseed petals and leaves by *Sclerotinia sclerotiorum* revealed by scanning electron microscopy. *Plant. Pathol.* **44**(1), 22–30 (1995).
19. Ghozlan, M. H., El-Argawy, E., Tokgoz, S., Lakshman, D. K. & Mitra, A. Plant defense against necrotrophic pathogens. *Am. J. Plant Sci.* **11**, 2122–2138 (2020).
20. Kamle, M., Borah, R., Bora, H., Jaiswal, A. K., Singh, R. K. & Kumar P. Systemic acquired resistance (SAR) and induced systemic resistance (ISR): Role and mechanism of action against phytopathogens. In *Fungal Biotechnology and Bioengineering*. 457–470 (Springer, 2020).
21. Shen, Q., Liu, L., Wang, L. & Wang, Q. Indole primes plant defense against necrotrophic fungal pathogen infection. *PLoS ONE* **13**(11), e0207607 (2018).
22. Vlot, A. C. *et al.* Systemic propagation of immunity in plants. *New Phytol.* **229**(3), 1234–1250 (2021).
23. Allan, J. *et al.* The host generalist phytopathogenic fungus *Sclerotinia sclerotiorum* differentially expresses multiple metabolic enzymes on two different plant hosts. *Sci. Rep.* **9**, 19966 (2019).
24. Seifbarghi, S. *et al.* Changes in the *Sclerotinia sclerotiorum* transcriptome during infection of *Brassica napus*. *BMC Genom.* **18**, 266 (2017).
25. Bolton, M. D., Thomma, B. P. & Nelson, B. D. *Sclerotinia sclerotiorum* (Lib.) de Bary: Biology and molecular traits of a cosmopolitan pathogen. *Mol. Plant Pathol.* **7**(1), 1–16 (2006).
26. Fagundes-Nacarath, I. R. F., Debona, D. & Rodrigues, F. A. Oxalic acid-mediated biochemical and physiological changes in the common bean-*Sclerotinia sclerotiorum* interaction. *Plant Physiol. Biochem.* **129**, 109–121 (2018).
27. Lyu, X. *et al.* A small secreted virulence-related protein is essential for the necrotrophic interactions of *Sclerotinia sclerotiorum* with its host plants. *PLoS Pathog.* **12**, e1005435 (2016).
28. Walker, P. L. *et al.* Tissue-specific mRNA profiling of the *Brassica napus*-*Sclerotinia sclerotiorum* interaction uncovers novel regulators of plant immunity. *J. Exp. Bot.* **73**(19), 6697–6710 (2022).
29. Ngou, B. P. M., Ahn, H.-K., Ding, P. & Jones, J. D. Mutual potentiation of plant immunity by cell-surface and intracellular receptors. *Nature* **592**, 110–115 (2021).
30. Guo, X. & Stotz, H. U. Defense against *Sclerotinia sclerotiorum* in *Arabidopsis* is dependent on jasmonic acid, salicylic acid, and ethylene signaling. *Mol. Plant Microbe Interact.* **20**, 1384–1395 (2007).
31. Waduwara-Jayabahu, I. *et al.* Recycling of methylthioadenosine is essential for normal vascular development and reproduction in *Arabidopsis*. *Plant Physiol.* **158**(4), 1728–1744 (2012).
32. Valdés-Santiago, L. & Ruiz-Herrera, J. Stress and polyamine metabolism in fungi. *Front. Chem.* **1**, 42 (2014).
33. McCaghey, M. *et al.* Host-induced gene silencing of a *Sclerotinia sclerotiorum* oxalacetate acetylhydrolase using bean pod mottle virus as a vehicle reduces disease on soybean. *Front. Plant Sci.* **12**, 677631 (2021).
34. Wu, J. *et al.* Host-induced gene silencing of multiple pathogenic factors of *Sclerotinia sclerotiorum* confers resistance to *Sclerotinia* rot in *Brassica napus*. *Crop J.* **10**(3), 661–671 (2022).
35. Wang, M. *et al.* Bidirectional cross-kingdom RNAi and fungal uptake of external RNAs confer plant protection. *Nat. Plants.* **2**, 16151 (2016).
36. Wytinck, N., Manchur, C. L., Li, V. H., Whyard, S. & Belmonte, M. F. dsRNA uptake in plant pests and pathogens: Insights into RNAi-based insect and fungal control technology. *Plants.* **9**(12), 1780 (2020).
37. Girard, I. J. *et al.* RNA sequencing of *Brassica napus* reveals cellular redox control of *Sclerotinia* infection. *J. Exp. Bot.* **68**(18), 5079–5091 (2017).
38. Uloth, M. B., Clode, P. L., You, M. P. & Barbetti, M. J. Attack modes and defence reactions in pathosystems involving *Sclerotinia sclerotiorum*, *Brassica carinata*, *B. juncea* and *B. napus*. *Ann. Bot.* **117**(1), 79–95 (2016).
39. Young, C. S. & Werner, C. P. Infection routes for *Sclerotinia sclerotiorum* in apetalous and fully petalled winter oilseed rape. *Plant. Pathol.* **61**(4), 730–738 (2011).
40. Davidson, A. L., Blahut-Beatty, L., Itaya, A., Zhang, Y. & Zheng, S. D. Histopathology of *Sclerotinia sclerotiorum* infection and oxalic acid function in susceptible and resistant soybean. *Plant. Pathol.* **65**(6), 878–887 (2016).
41. Rana, K. *et al.* *Sclerotinia sclerotiorum* Thioredoxin1 (SsTrx1) is required for pathogenicity and oxidative stress tolerance. *Mol. Plant Pathol.* **11**, 1413–1426 (2021).
42. Gao, Q. M., Zhu, S., Kachroo, P. & Kachroo, A. Signal regulators of systemic acquired resistance. *Front. Plant Sci.* **6**, 228 (2015).
43. Kinkema, M., Fan, W. & Dong, X. Nuclear localization of NPR1 is required for activation of PR gene expression. *Plant Cell* **12**, 2339–2350 (2000).
44. Kumar, P. *et al.* Pivotal role of bZIPs in amylose biosynthesis by genome survey and transcriptome analysis in wheat (*Triticum aestivum* L.) mutants. *Sci. Rep.* **8**, 17240 (2018).
45. Backer, R., Naidoo, S. & van den Berg, N. The NONEXPRESSOR OF PATHOGENESIS-RELATED GENES 1 (NPR1) and related family: Mechanistic insights in plant disease resistance. *Front. Plant Sci.* **10**, 102 (2019).
46. Noshi, M., Mori, D., Tanabe, N., Maruta, T. & Shigeoka, S. *Arabidopsis* clade IV TGA transcription factors, TGA10 and TGA9, are involved in ROS-mediated responses to bacterial PAMP flg22. *Plant Sci.* **252**, 12–21 (2016).
47. Wei, Y., Liu, G., Chang, Y., He, C. & Shi, H. Heat shock transcription factor 3 regulates plant immune response through modulation of salicylic acid accumulation and signalling in cassava. *Mol. Plant Pathol.* **19**(10), 2209–2220 (2018).

48. Cui, H. *et al.* A core function of EDS1 with PAD4 is to protect the salicylic acid defense sector in *Arabidopsis* immunity. *New Phytol.* **213**(4), 1802–1817 (2017).
49. Khan, A., Khan, V., Pandey, K., Sopory, S. K. & Sanan-Mishra, N. Thermo-priming mediated cellular networks for abiotic stress management in plants. *Front. Plant Sci.* **13**, 866409 (2022).
50. Qu, A. L., Ding, Y. F., Jiang, Q. & Zhu, C. Molecular mechanisms of the plant heat stress response. *Biochem. Biophys. Res. Commun.* **432**(2), 203–207 (2013).
51. András, N. *et al.* The mitogen-activated protein kinase 4-phosphorylated heat shock factor A4A regulates responses to combined salt and heat stresses. *J. Exp. Bot.* **70**(18), 4903–4918 (2019).
52. Pérez-Salamó, I. *et al.* The heat shock factor A4A confers salt tolerance and is regulated by oxidative stress and the mitogen-activated protein kinases MPK3 and MPK6. *Plant Physiol.* **165**(1), 319–334 (2014).
53. Wang, Z. *et al.* Recent advances in mechanisms of plant defense to *Sclerotinia sclerotiorum*. *Front. Plant Sci.* **10**, 1314 (2019).
54. Shao, D., Smith, D. L., Kabbage, M. & Roth, M. G. Effectors of plant necrotrophic fungi. *Front. Plant Sci.* **12**, 687713 (2021).
55. Rajarammohan, S. Redefining plant-necrotroph interactions: The thin line between hemibiotrophs and necrotrophs. *Front. Microbiol.* **12**, 673518 (2021).
56. Höch, K., Koopmann, B. & von Tiedemann, A. Lignin composition and timing of cell wall lignification are involved in *Brassica napus* resistance to stem rot caused by *Sclerotinia sclerotiorum*. *Phytopathology* **111**(8), 1438–1448 (2021).
57. Valdés-Santiago, L., Cervantes-Chávez, J. A., León-Ramírez, C. G. & Ruiz-Herrera, J. Polyamine metabolism in fungi with emphasis on phytopathogenic species. *J. Amino Acids* **2012**, 837932 (2012).
58. McLoughlin, A. G. *et al.* Developing new RNA interference technologies to control fungal pathogens. *Can. J. Plant Path.* **40**(3), 325–335 (2018).
59. Good, R. T. *et al.* OfftargetFinder: A web tool for species-specific RNAi design. *Bioinformatics* **32**(8), 1232–1234 (2016).
60. Mbengue, M. *et al.* Emerging trends in molecular interactions between plants and the broad host range fungal pathogens *Botrytis cinerea* and *Sclerotinia sclerotiorum*. *Front. Plant Sci.* **7**, 422 (2016).
61. Reich, J., Chatterton, S. & Johnson, D. Temporal dynamics of *Botrytis cinerea* and *Sclerotinia sclerotiorum* in seed alfalfa fields of southern Alberta, Canada. *Plant Dis.* **101**(2), 331–343 (2017).
62. Logemann, E., Birkenbihl, R. P., Ülker, B. & Somssich, I. E. An improved method for preparing *Agrobacterium* cells that simplifies the *Arabidopsis* transformation protocol. *Plant Methods* **2**, 16 (2006).
63. Livak, K. J. & Schmittgen, T. D. Analysis of relative gene expression data using real-time quantitative PCR and the 2^{(-Delta Delta C(T))} Method. *Methods* **4**, 402–408 (2001).
64. Ziegler, D. J., Khan, D., Kalichuk, J. L., Becker, M. G. & Belmonte, M. F. Transcriptome landscape of the early *Brassica napus* seed. *J. Integr. Plant Biol.* **61**(5), 639–650 (2019).
65. Bolger, A. M., Lohse, M. & Usadel, B. Trimmomatic: A flexible trimmer for illumina sequence data. *Bioinformatics* **30**, 2114–2120 (2014).
66. Kim, D., Langmead, B. & Salzberg, S. L. HISAT: A fast spliced aligner with low memory requirements. *Nat. Methods* **12**, 357–360 (2015).
67. Liao, Y., Smyth, G. K. & Shi, W. featureCounts: An efficient general purpose program for assigning sequence reads to genomic features. *Bioinformatics* **30**(7), 923–930 (2014).
68. Becker, M. G., Walker, P. L., Pulgar-Vidal, N. C. & Belmonte, M. F. SeqEnrich: A tool to predict transcription factor networks from co-expressed *Arabidopsis* and *Brassica napus* gene sets. *PLoS ONE* **12**(6), e0178256 (2017).

Acknowledgements

The authors would like to thank Dr. Odile Carisse, Agriculture and Agri-Food Canada for *Botrytis cinerea* spores, Dr. Khalid Rashid, Agriculture and Agri-Food Canada for *S. sclerotiorum* spores, and Genome Quebec CES facility for processing cDNA libraries and providing raw mRNA sequencing data.

Author contributions

P.L.W., M.F.B., S.W. conceptualized and designed the study. A.M., D.K. and V.H. generated transgenic Arabidopsis. P.L.W. and S.G. performed infection assays and RT-qPCR analysis. D.Z. performed microscopy. P.L.W. and J.W. generated cDNA libraries for RNA sequencing. P.L.W. performed sequencing data analysis. P.L.W. wrote the manuscript. M.F.B. and S.W. supervised the study and contributed to the editing of the manuscript.

Funding

This work was generously supported by grants from the province of Manitoba Agricultural Rural Development Initiative, the Canola Council of Canada, and the Western Grains Research Foundation to SW and MFB. PLW was supported by a Manitoba Graduate Fellowship.

Competing interests

The authors declare no competing interests.

Additional information

Supplementary Information The online version contains supplementary material available at <https://doi.org/10.1038/s41598-023-33335-4>.

Correspondence and requests for materials should be addressed to M.F.B.

Reprints and permissions information is available at www.nature.com/reprints.

Publisher's note Springer Nature remains neutral with regard to jurisdictional claims in published maps and institutional affiliations.



Open Access This article is licensed under a Creative Commons Attribution 4.0 International License, which permits use, sharing, adaptation, distribution and reproduction in any medium or format, as long as you give appropriate credit to the original author(s) and the source, provide a link to the Creative Commons licence, and indicate if changes were made. The images or other third party material in this article are included in the article's Creative Commons licence, unless indicated otherwise in a credit line to the material. If material is not included in the article's Creative Commons licence and your intended use is not permitted by statutory regulation or exceeds the permitted use, you will need to obtain permission directly from the copyright holder. To view a copy of this licence, visit <http://creativecommons.org/licenses/by/4.0/>.

© The Author(s) 2023